8 Design of Novel Coatings

8.1 Coating Requirements

Thermally sprayed and PVD/CVD coatings must be carefully designed to obtain maximum performance for the required application. An initial example will be given based on the concept of advanced layered coatings for cutting tools [1]. Even though it relates predominantly to thin PVD or CVD coatings the strategy can also be applied, in principle, to thick thermally sprayed coatings [2].

- Coatings for cutting tools can:

- improve service life of the tool, i.e. reduce the frequency of tool changes,
- provide more favorable operating conditions, i.e. higher speed and feed rates and thus improve the economy of the cutting and milling operations,
- provide higher product quality, i.e. better surface finish and tighter tolerances,
- open up new areas of applications, i.e. machining of difficult to handle non-metallic materials such as wood, plastic and composites, and
- achieve resource conservation, i.e. reduced materials losses and machining of more economical materials.

There are, however, conflicting basic requirements for coating performances. The hard coating materials in question are frequently oxide ceramics such as Al_2O_3 and Cr_2O_3, or nonoxide ceramics such as transition metal carbides (TiC, TaC, WC, Mo_2C), nitrides (TiN, Si_3N_4, SiAlONs) and borides (TiB_2). There are three problems.

1. Ceramic coatings must have good adhesion to the metallic substrate, but little tendency to react with the material of the metal chip removed by the tool from the workpiece. This is particularly important when at high cutting speeds and therefore high frictional temperatures the material of the coating dissolves in the chip.
2. The ceramic constitutes of a hard layer with a high melting point, but there should be little crack propagation, i.e. high fracture toughness of the coating is required.
3. The ceramic layer must be hard and high melting, but good adhesion is needed under widely changing temperature conditions imposed by friction and intense shear forces at the worked interface, and the associated high thermal stresses and high thermal expansion [1].

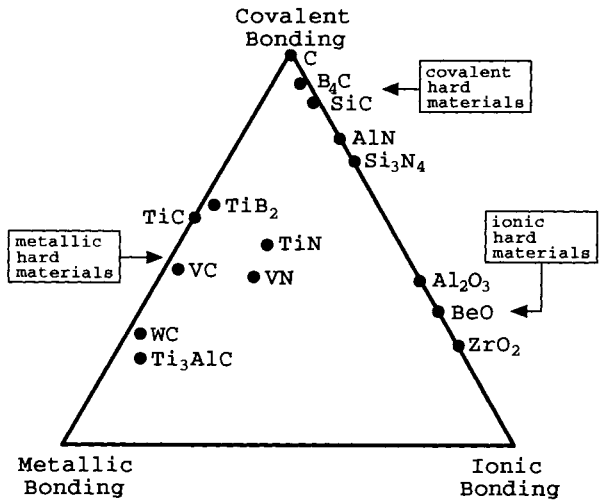

Figure 8-1. Chemical bonding types of different hard ceramic materials [1].

A way to look at the compatibility of different ceramic materials is through their differing chemical bonding type (Fig. 8-1). Metallic hard materials, such as WC, TiC or TiB_2 are characterized by their high proportion of metal–metal bonds in the f.c.c. closed-packed arrangement of metal atoms, whereas the small carbon or boron atoms occupy the octahedral interstitial sites. On the other hand, covalent ceramic materials have a high proportion of highly directional covalent bonds, and heteropolar (ionic) ceramic materials possess simple sublattices of large close-packed oxygen anions with the small metal atoms at interstitial sites, opposite to the metal bonding structure.

In general, all materials used for protective layers are characterized by mixed bonding types. Their properties change with the position of the material in the bonding triangle (Fig. 8-1). TiN close to the centre of the triangle has a particularly favorable combination of metallic, covalent and ionic bonding types. Carbide, nitrides and borides of the transition metals (Ti, V, W) crystallize in simple, densely packed lattices of large metal atoms with the non-metallic atoms joined to the metal lattice by covalent or mixed covalent/ionic bonds. If metallic and ionic structures are combined, i.e. TiC–Al_2O_3, there are no corresponding metal planes at the interface but the Ti-planes of TiC will match the oxygen planes of Al_2O_3 in positioning and size. Because the covalent structures have highly directional, saturated bonds, there is only a small tendency to interact with other materials at the interface.

8.2 Design of Novel Advanced Layered Coatings

The concept of 'advanced layers' includes the design [1] of:

- gradient layers [2],
- layer materials in thermodynamic equilibrium,

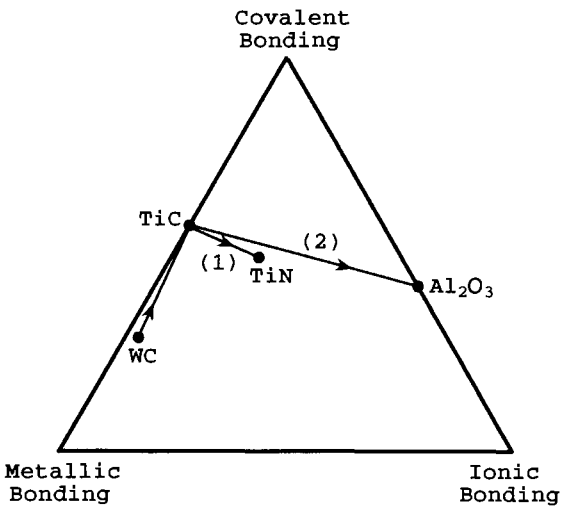

Figure 8-2. Possible designs of gradient-layer coatings WC–TiC–TiN (1) and WC–TiC–Al_2O_3 (2) [1].

- extended solid solution, and
- multilayers.

8.2.1 Gradient Layers

Functional gradient materials (FGMs) display continuously (or discontinuously) varying compositions or microstructures over definable geometric distances [2].

Very thin layers can be deposited by PVD techniques. Such coatings are designed so that to the substrate is first added an adhesive layer with a large fraction of metal bonds. These bonds tend to form a stable external layer with little tendency to interact. Examples are given in Fig. 8-2 of a gradient layer combination WC–TiC–TiN (1) and WC–TiC–Al_2O_3 (2). Such gradient layer coatings for cutting tools will exhibit superior flank wear resistance. In fact, the wear depth of uncoated WC during interrupted cutting is reduced by using a PVD TiC–TiN gradient coating from $> 160\,\mu m$ to a minimum wear depth of $20\,\mu m$ [1]. These data were obtained from interrupted cutting conditions of CK 45 (speed: $125\,m\,min^{-1}$, feed: 0.2 mm per revolution, depth of cut: 2 mm, cutting time: 5 min; corresponding to 3500 impacts).

Plasma-spray processing offers an alternative way to deposit FGMs in a flexible and economical manner. It is possible to deposit multiple constituents simultaneously, for example to produce thermal barrier graded layers with enhanced survivability for gas turbines and diesel engines. Gradient layers are primarily employed to reduce discontinuities in the coefficients of thermal expansion to avoid mismatch-related failure in service. Such discontinuities frequently result in fatal cracks and spallation at the sharp interface between the substrate and a thermal barrier coating. FGMs are capable of spreading out this mismatch stress and thus reduce crack initiation. Equipment to deposit FGMs can be classified as: single plasmatron–multiple powder feeders with blended or composite powders; multiple plasmatron–independent feeding systems for each components; and process combinations–wire/powder feed systems combinations. Using a single plasmatron–dual feeder combination, a

graded NiCrAl/Y–PSZ coating has been produced with an almost linear increase of Y–PSZ as a function of the distance from the interface to the substrate. The microstructure of this 2 mm thick gradient coating was composed of 70 μm-thick discrete layers of varying compositions [2]. Likewise, the elastic modulus of such a gradient coating decreased nearly linearly with increasing Y–PSZ content, i.e. away from the interface [3]. Despite these advances the benefits of grading for stress relaxation need to be studied in detail in the context of other coating characteristics such as environmental stability and manufacturing complexity.

8.2.2 Layered Materials in Thermodynamic Equilibrium

In the structurally compatible systems TiC/TiN or TiC/VN (see Fig. 8-1), extended formation of solid solution takes place that can either lead to a single phase solid solution, or, at lower temperature, to the decomposition of this single phase into two phases with added particle strengthening due to mechanical reinforcement.

8.2.3 Extended Solid Solution

In structurally noncompatible ceramics (TiN/AlN, TiC/SiC) with different bonding types an equilibrium solid solution is not possible for metastable layer materials composed of a metallic and a covalent hard material. Rapid solidification may lead to extended metastable solid solution over the entire compositional range.

8.2.4 Multilayers

Fine-grained multiphase structures with many phase boundaries frequently produce structures with increased toughness. Limited crack propagation takes place in the modulated layer structure because of deflection and arrest of cracks at the interfaces due to many oscillations between tensile and compressive stresses. PVD methods are ideally suited to produce TiC/TiB_2, TiC/TiN or TiN/TiB_2 composite coatings with up to 500 individual layers with a total layer thickness not exceeding 5 μm. The advantage of the multilayer concept lies in the reduction of grain growth, the introduction of many interfaces, and the formation of modulated layer material that changes the mechanical properties, and leads to effective stopping of crack propagation. The application of various coating technologies to the design of novel coatings are shown in Table 8-1.

8.3 Principles of Statistical Design of Experiments

8.3.1 The Experimental Environment and its Evolution

A brief survey of the techniques of statistical design of experiments (SDE) most frequently applied to thermally sprayed coatings has been given by Bisgaard [4] and

Table 8-1. Design of surface coatings.

Layer materials concept	Coating technology
Solid solution coatings	PS, LPPS, CVD, PACVD, PVD
Gradient coatings	PS, LPPS, CVD, PACVD, PVD
Multilayers	PVD, CVD, (PACVD)
Metastable layer materials	PVD, (PACVD)
Multiphase layer materials	PVD, (CVD, PACVD, PS, LPPS)

PS = plasma spraying; LPPS = low-pressure plasma spraying; CVD = chemical vapor deposition; PACDV = plasma-assisted chemical vapor deposition; PVD = physical vapor deposition (magnetron sputtering, ion plating, arc evaporation).

Heimann [5]. Two-level factorial analysis applied to plasma spraying was reviewed by Lugscheider and Knepper [6]. The design methodologies are based on the ideas of Plackett and Burman [7], Box [8, 9], Deming [10] and Taguchi [11]. Software is available to perform the statistical calculations required with ease [12].

According to Tukey [13], industrial experiments can be classified according to their depths of intellectual investment as: confirmation experiments; exploration experiments; and fundamental or 'stroke-of-genius' experiments. A second method of classification is based on the distance of their objective from the real world, i.e. from the market [14]. Finally, the continuity of factors provides a third classification scheme. If the factors (parameters, variables) are continuous and controllable at preset levels, then the response surface methodology is the method of choice. If, however, some factors are orderable but not measurable, i.e. at discrete levels, the response surface analysis becomes less useful and should be replaced by nested or split-plot designs [15]. At a lower level of predicting power, screening designs like Plackett–Burman designs [7] that can handle mixtures of continuous and discrete factors are particularly important as a statistical experimental design for the optimization of plasma sprayed coatings (see Secs. 8.3.2, 8.4.1).

Every experiment attempts to approximate the 'real world' in some ways but must avoid, by a set of simplifying assumptions, the complex interactions occuring in real systems. There are, in principle, two ways to accomplish this: the *'classical' experimental strategy* that varies one parameter at a time but attempts to keep all others constant, and the *statistical strategy* that varies factors simultaneously to obtain a maximum of information with a minimum number of experiments. Thus the experimental economy becomes the overriding principle of the strategy. The classical experimental strategy yields accurate results but requires many experiments, and may give misleading conclusions to problems that have synergistic factor interactions, and also fails to elucidate the 'structure' of a system. Table 8-2 compares these two strategies [16].

8.3.1.1 Screening Designs

The evolution of the experimental environment usually starts with a screening design, for example a Plackett–Burman [7] or Taguchi design [11] with many indepen-

Table 8-2. Two viewpoints of the 'real world' [16].

	Classical	Statistical
Number of runs	many	few
Type of response	complex	simple
Synergism	absent	present
Error	small	large
Strategy	one-factor-at-a-time	factorial
Thought pattern	vertical	lateral [17]

dent (up to 40) variables. It yields a rather crude prediction of the relative magnitude and sign of the parameters and thus the ranking of importance of parameters through a first-order polynomial model. The experimenters should list and investigate carefully all possible parameters they can think of but should refrain from skipping some because of 'folklore', laboratory gossip, or preferences and hunches. The penalty for the tremendous reduction in the number of required experiments, however, will be the failure to detect synergistic interactions between parameters. On the other hand, an advantage of the screening designs is that they can accommodate a mix of continuous and discrete parameters. Plackett–Burman designs are *saturated*, i.e. they contain as many experimental runs as there are coefficients to determine in the first-order polynomial model. If the number of potential influencing factors is very large, *supersaturated* designs can be selected that contain less runs than coefficients to be estimated [18]. An even more reduced design plan can be obtained using the principle of chance balance [18, 19]. More modern approaches consider evolutionary algorithms combined with fuzzy logic that allow estimation of the behavior of a complex system with but a few randomly chosen tests.

8.3.1.2 Response Surface Designs

With the independent parameters (up to eight) identified by screening designs to significantly influence the response of the dependent parameter(s), a 'limited response surface' experiment should be run such as a full two-level factorial, 2^p or even a fractional three-level factorial (Box–Behnken) design [8] that yields higher quality predictions by allowing interpolation within the experimental space by a second-order polynomial model. Such a model determines nonlinear behavior, i.e. the curvature of the response surface and thus permits the estimation of synergistic parameter interactions.

8.3.1.3 Theoretical Models

The polynomial models approximate the 'true' response surface only in the necessarily narrow region of the investigated parameter space. Thus, any extrapolation beyond the proven validity of the predictions is dangerous and may lead to useless or even nonsensical results. To avoid this, eventually theoretical models have to be built

Figure 8-3. Saturated Plackett–Burman design for estimation of 11 parameters with 12 runs.

Run	x_1	x_2	x_3	x_4	x_5	x_6	x_7	x_8	x_9	x_{10}	x_{11}
1	+	−	+	−	−	−	+	+	+	−	+
2	+	+	−	+	−	−	−	+	+	+	−
3	−	+	+	−	+	−	−	−	+	+	+
4	+	−	+	+	−	+	−	−	−	+	+
5	+	+	−	+	+	−	+	−	−	−	+
6	+	+	+	−	+	+	−	+	−	−	−
7	−	+	+	+	−	+	+	−	+	−	−
8	−	−	+	+	+	−	+	+	−	+	−
9	−	−	−	+	+	+	−	+	+	−	+
10	+	−	−	−	+	+	+	−	+	+	−
11	−	+	−	−	−	+	+	+	−	+	+
12	−	−	−	−	−	−	−	−	−	−	−

[9, 20] that yield the exact mathematical response surface, usually by the application of first-order differential equations.

8.3.2 Screening Designs

In a real experimental program the screening designs, in particular Plackett–Burman designs are the starting point for any investigation of a completely unknown system. They are designed to screen out the few really important variables from a large number of possible ones with a minimum of test runs. Plackett–Burman designs are fractions of an $N = 2^p$ factorial for which N is a multiple of 4. Although they allow a tremendous reduction in experimentation there is no estimate of synergistic nonlinear parameter interactions. In fact, only estimates of main effects clear of each other can be obtained. A saturated Plackett–Burman design useful for optimization of 11 plasma spray parameters in only 12 runs is shown in Fig. 8-3. The '+'-signs are assigned to the parameters x_i at their maximum levels, the '−'-signs to their minimum levels. The factor effects are calculated by adding in each column the '+'-responses ($\sum +$) and subtracting the sum of the '−'-responses ($\sum -$). The value $\Delta = (\sum +) - (\sum -)$, divided by the number of '+'-(or '−')-signs in the columns with assigned factors is the factor effect for the parameter x_i. For the extra columns to which no factors have been assigned this 'factor effect' is an estimate of the experimental error. For example, assignment of only six variables, x_1 to x_6 leaves five degrees of freedom, i.e. unassigned factor effects x_7 to x_{11} that can be used to estimate the standard deviation of the factor effects, $\sigma_{FE} = \{(1/q)\sum x_{iq}^2\}^{1/2} = \{(1/n)\sum E_i^2\}^{1/2}$.

To determine which factors x_i are statistically significant the calculated factor effects are being compared with the minimum factor significance, {min}. The minimum significant factor effect is

$$\{\min\} = t_\nu^\alpha \sigma_{FE}, \tag{8-1}$$

with t_ν^α = Student's t for ν degrees of freedom, and α level of confidence for a double-sided t-distribution. All factors whose effects are larger than the (absolute) value of {min} are considered statistically significant. An example for the application of a Plackett–Burman screening test is given in Sec. 8.4.1. Although Plackett–Burman designs are available for nearly any multiple of four trials, the most useful ones are for 12, 20 or 28 trial runs. Such designs handle nominally 11, 19 and 27 factors, respectively. It is good practice to conduct an operability review after having selected any p columns for factors. For increased precision of prediction, a larger design could be used and/or a reflected design could be added [7]. By using the next larger design partial replication is obtained. For example, with 6 factors, the recommended design has 12 runs. This leaves 5 degrees of freedom for estimation of the experimental error. Alternatively, the 6 factors can be run in a 20 trial design, hence leaving 13 degrees of freedom for estimation of the experimental error. Reflected designs are able to estimate main effects (almost) clear of two-factor interactions, and thus approach the predicting power of fractional factorial designs (see below).

The selection of the level of significance, α, requires some discussion. When there is only a relatively small number of degrees of freedom, i.e. when a low number of runs has been performed, it is preferable to select a significance level lower than 0.95. In this case, the 'power of test' is greater, i.e. the likelihood of detecting a significant factor effect if it exists. As a rule of thumb, for degrees of freedom ≤ 5, 5 to 30, and ≥ 30, respectively, significance levels of 0.90, 0.95, and 0.99, respectively should be picked.

If two-factor interactions are present, Plackett–Burman designs have the desirable property that significant factor effects stand out over a pool of background noise containing both experimental error and interactions when present. In the absence of interactions, the *precision ratio* achieved is

$$\sigma_{FE}/\sigma = 2/n^{1/2}, \tag{8-2}$$

where σ_{FE} = standard deviation of a factor effect, σ = standard deviation of a single observation, and n = total number of observations (runs) in the selected design. The value of n, i.e. the number of experimental runs should be large enough to have a high probability of separating the significant signal from experimental noise, but small enough the optimize time and costs. The size of the factor effect to be detected is Ω, and the desired probability that a significant parameter can be detected when it has a true effect of size Ω, is $(1 - \beta) \geq 0.90$. This is satisfied if $\sigma_{FE} = \Omega/4$. From (8-2) it follows that

$$n = (8\sigma/\Omega)^2 = [8/(\Omega/\sigma)]^2, \tag{8-3}$$

with Ω/σ = signal-to-noise ratio.

Eq. (8-3) is called Wheeler's test. To detect effects twice as large as the experimental error ($\Omega = 2\sigma$), n must be 12 to 16. To detect effects the same size as the error ($\Omega = \sigma$), n becomes four times as large, i.e. 48 to 64. Weak factor effects thus require a large number of experiments.

8.3.3 Factorial Designs

8.3.3.1 Full Factorial Designs

Factorial designs permit the estimation of the main (linear) effects of several factors, x_i simultaneously and clear of two-factor interactions, $\{x_i x_j\}$. The total number of experiments, N is obtained by running experiments at all combinations of the p factors with l levels per factor, i.e. $N = l^p$ for a full factorial design. In particular, two-level factorial designs ($l = 2$) are highly useful for a wide variety of problems. They are easy to plan and to analyse, and readily adaptable to both continuous and discrete factors. Such designs provide adequate prediction models for responses without a strong nonlinear behavior in the experimental region. However, for best results the responses Y should be continuous, and have uniform and independent errors. This means that: the experimental error must have approximately the same magnitude at all experimental points; and the size and sign of error at any one experimental point must not be affected by the sizes and signs of errors that occur at other experimental points. If the first requirement cannot be guaranteed a logarithmic transformation of the responses Y is often advisable. With factor coding as discussed above, using the so-called Yates order [21] and randomization of the experimental trials, factor effects for each main effect and two-factor interaction are calculated similarly to the procedure mentioned in Sec. 8.3.2. The computation of factor effects and residuals can also be quickly and accurately accomplished using the inverse Yates algorithm, [22]. The test of significance can be derived from an appropriate t-test:

$$\{\min\}_{\text{lin}} = t_\nu^\alpha \sigma_{\text{FE}} (2/mk)^{1/2}, \tag{8-4a}$$

$$\{\min\}_{\text{c}} = t_\nu^\alpha \sigma_{\text{FE}} (1/mk + 1/c)^{1/2}, \tag{8-4b}$$

where $\{\min\}_{\text{lin}}$, $\{\min\}_{\text{c}}$ are the minimum significant factor effects for linear effects and curvature, respectively, and $m = 2^{p-1}$ for factor effects and 2^p for the average, $k =$ number of replicates, and $c =$ number of center points. If a computed factor effect is larger (in absolute value) than $\{\min\}_{\text{lin}}$ than it can be safely concluded that the true effect Ω is nonzero. Also, when the curvature effect is larger than $\{\min\}_{\text{c}}$ then at least one factor has nonzero curvature associated with it. Applications of full factorial designs 2^3 to the design of (Ti, Mo)C–NiCo– and 88WC12Co–coatings on mild steel, and a 2^5 design applied to a self-fluxing NiCr coating on steel will be dealt with in Sec. 8.4.2.

8.3.2.2 Fractional Factorial Designs

If the number of parameters p to be estimated becomes larger than, say 5 a full factorial may not be appropriate anymore for reasons of experimental economy. Then fractions of a full factorial can be run, i.e. $N = 2^{p-q}$. In particular, half-fraction of full factorials, $N = 2^{p-1}$ estimate main effects and two-factor interactions clear of each other.

Fractional factorial designs are useful in the following situations [23]:

1. when some interactions can be reasonably assumed nonexistent from prior knowledge,
2. in screening operations where it is expected that the effects of all but a few of the factors will be negligible,
3. where blocks of experiments are run in sequence, and ambiguities remainining at an earlier stage of experimentation can be resolved by later blocks of experiments, and
4. when some factors that may interact are to be studied simultaneously with others whose influence can be described through main effects only.

Fractional factorial designs can be divided into three types with regard to their *power of resolution*, i.e. their degree of fractionation. The higher the degree of fractionation the more comprehensive the assumptions required to arrive at unequivocal interpretation of the system. Designs of resolution III, for eaxmple 2^{3-1}, are those in which no main effect is confounded with any other main effect, but main effects are confounded with two-factor interactions, and two-factor interactions with each other. In designs of resolution IV, for example 2^{4-1}, no main effect is confounded with any other main effect or two-factor interaction, but two-factor interactions are confounded with each other. Finally, in designs of resolution V, for example 2^{5-1}, no main effect or two-factor interaction is confounded with any other main effect or two-factor interaction, but two-factor interactions are confounded with three-factor interactions. Since in most real problems three- and higher-factor interactions can be safely neglected, a design of resolution V should be the design of choice. However, in order to reduce the number of runs required and thus keep within the economical bounds of most research and development projects, fractional factorial designs of resolution IV can be tolerated. The design 2^{8-4} discussed in Sec. 8.4.3 is of resolution IV. The confounding of two-factor interactions in this design leads to composite two-factor interaction, i.e. the sum of four two-factor interactions. Examples of these fractional factorial designs applied to 88WC12Co-, Ti-, $97Al_2O_33TiO_2$-, 85Fe15Si- and stellite coatings on mild and austenitic steel substrates will be shown in Sec. 8.4.3.

8.3.4 Box–Behnken Designs

Box–Behnken designs [8] are incomplete three-level factorial designs that allow estimation of the coefficients in a second-degree graduating polynomial. They employ subsets of the corresponding full three-level factorial, 3^p. For example, the three-factor design uses only 13 of the 27 points of the full factorial 3^3 with two extra replicates of the center points added, for a total of 15 experimental points of a spherical space-filling[1] and rotatable design. Another desirable feature of such designs with

[1] Note that the factorial designs are considered to have a 'cuboidal' or 'hypercube' factor space whereas the true response surface designs have a 'spherical' factor space.

$p > 4$ is the possibility to run it in separate blocks of points. Such *orthogonal blocking* permits subtraction of the effect of a shift of response between blocks, and thus removal of bias errors due to differences in extraneous variables not considered in the design. The 15 data points in the three-factor Box–Behnken design are five more than the minimum number of 10 required to estimate the coefficients of the design (3 linear main effects, 3 parabolic main effects, 3 two-factor effects, and 1 three-factor effect). Thus it provides five degrees of freedom for error. Orthogonal blocking is possible for designs from four up to ten factors. Rotatability is associated with the geometric properties of the design, i.e. the arrangement of the array of data points, except for the center point, to be at the mid-points of the edges or faces of a hypercube whose dimensionality is given by the number of factors considered. Hence all points are situated on a single sphere and are thus equidistant from the center. This means that the design is balanced by the mathematical momentum condition. The replicated center point allows estimation of the minimum factor significance, i.e. the inherent experimental error, and prediction of constant variances as a function of distance from the center.

It is good experimental strategy to employ such Box–Behnken-type designs at a rather advanced stage of experimentation when the number of potentially significant factors has been narrowed down to 3 to 6 continuous factors. As clearly pointed out by Bisgaard [4] even considering nonlinearity of responses in plasma-sprayed designs does not warrant, for reasons of experimental economy, three-level factorial designs in the initial stage of experimentation. Thus second-order effects should be dealt with exclusively when they actually show up in the set of data, and not only because the experimenter suspects that the system under investigation may show some global nonlinearity! When switching from two- to three-level designs any discrete, i.e. non-continuous factor effect must be considered constant. The response surface obtained through a Box–Behnken response surface design provides usually a high-quality prediction over a region where linear, parabolic (curvature) and two-factor interactions are needed to describe a response of the system, Y as a function of the coefficients of the independent input parameters X_i obtained by a full quadratic polynomial for p independent parameters:

$$Y = b_0 + \sum b_j X_j + \sum b_{jj'} X_j X_{j'} + \sum b_{jj} X_j^2, \tag{8-5}$$

with $j > j'$.

8.3.5 Designs of Higher Dimensionality

Three levels are the minimum number for each factor to describe accurately nonlinear (curvature) effects. To add additional power of prediction to a Box–Behnken design, it is advisable to use more than three factor levels. One popular class of response surfaces are the *central composite* or Box–Wilson [24] designs that employ five levels for each factor. It is composed of a full two-level factorial 2^3 with added center points plus six star points outside the cube planes defined by the four points of the two-level factorial. The geometric shape of the resulting five-level design is a

tetrakishexahedron whose 14 design points surround a k-time replicated center point. This polyhedron is 'cuboidally' spacefilling and can be described as the dual polytope of a cuboctahedral Dirichlet domain (Voronoi polyhedron).

8.4 Optimization of Coating Properties: Case Studies

8.4.1 Plackett–Burman (Taguchi) Screening Designs

Optimization of a novel (Ti, Mo)C–NiCo coating on mild steel (German steel number St38) was performed by vacuum plasma-spraying in an argon/hydrogen plasma using a 12-point 11-factor Plackett–Burman design (L_{12}-type according to Taguchi) [25]. The six factors varied at two levels (high and low) were: **1** = powder (agglomerate) grain size[2], **2** = plasma power, **3** = powder feed rate, **4** = plasmatron traverse speed, **5** = chamber pressure, **6** = spray (stand-off) distance. The plasma power, **2**, was not an independent parameter but obtained by an appropriate selection of the argon/hydrogen ratio and the current. The low value of **2** was 42 kW (argon: 48 l min^{-1}, hydrogen: 6 l min^{-1}, current: 800 A), the high value was 47 kW (argon: 48 l min^{-1}, hydrogen: 7 l min^{-1}, current: 900 A). The remaining factors and their levels were: **1** ($-32 + 10$ μm; $-63 + 32$ μm), **3** (0.5; 1 scale), **4** (4 m min^{-1}; 8 m min^{-1}), **5** (80 mbar; 100 mbar), and **6** (340 mm; 380 mm). Four responses Y_i were measured: surface roughness of the deposit (Y_1), microhardness (Y_2), porosity (Y_3) and fracture energy density (Y_4). The factors found to influence those responses at a level of confidence of 95% were **1** (positive effect for surface roughness and porosity, negative effect for fracture energy density) and **6** (positive effect for porosity, negative effect for fracture energy density). In addition, with the parameters **2**, **5** and **6** a full factorial design 2^3 was run for the fine powder ($-32 + 10$ μm) with increased ranges of **2** (38 kW; 53 kW) and **5** (100 mbar; 180 mbar) and a reduced range of **6** (200 mm; 300 mm) in order to minimize the coating porosity. For the low levels of **2** (38 kW), **5** (100 mbar) and **6** (200 mm) a coating porosity around 2% could be achieved with reasonably low surface roughness and a fracture energy density around 30 J mm^{-3}. Problems occured with a high heat transfer to the substrate that requires efficient substrate cooling.

Other recently reported optimization studies on plasma-sprayed coatings based on L_8 or L_{16} Taguchi designs relate to:

- NiCrAl/bentonite abradable coatings (L_{16} design, 15 independent parameters, 3 dependent parameters: erosion resistance, tensile strength, hardness) [26]
- HVOF-sprayed Al–Si/polyester abradable coatings (L_8 design, 5 independent parameters, 3 dependent parameters: hot erosion resistance, bond strength, hardness) [27]

[2] Here and in the following text the factors X_1, $X_2 \ldots X_i$ will be denoted by **1**, **2**, ... ***i***.

- Thick thermal barrier coatings (TTBCs) (L_8 design, 7 independent parameters, 5 dependent parameters: erosion resistance, macrohardness, porosity, deposition efficiency, thermal shock resistance) [28]
- WC/Co-, Cr_3C_2/NiCr- and Al_2O_3/TiO_2 coatings (L_8 design, 7 independent parameters, 4 dependent parameters: microhardness, Rockwell macrohardness, tensile strength, composition) [29].

8.4.2 Full Factorial Designs

Such designs are not very common in the literature since they are limited to a rather small subset of spray parameters. Only if enough knowledge of the system under investigation has been accumulated such designs are being applied to fine-tune the parameters of a decreased factor space (see Sec. 8.4.1).

A two-level five-factor full factorial 2^5 was employed by Hurng *et al.* [30] to evaluate the properties of a self-fluxing nickel-base alloy containing 15 to 18 mass% Cr and 5 mass% (Fe + C + B + Si) deposited by a hybrid APS/PTA (plasma transferred arc) process on mild steel. The five independent parameters and their ranges were: **1** plasma current (420 A; 460 A), **2** spray distance (15 mm; 17 mm), **3** powder feed rate (8; 12 wheel speed units), **4** plasmatron traverse speed (25 mm s^{-1}; 35 mm s^{-1}) and **5** plasma transferred arc current (4;6 scale units). Each parameter setting was repeated thus giving two sets A and B of 32 runs each. In addition, 15 experiments were run at the 'working point', i.e. the midpoint between the low and high values selected for each parameter.

The optimized dependent response parameters were the microhardness ($800 \pm 40\,HV_{0.3}$), the porosity ($2.1 \pm 1.5\%$) and an oxide content as low as 0.13%. The significant parameters for optimizing the microhardness were the plasma current **1** with an effect per unit of $-0.83\,HV_{0.3}$ per A, the two-factor interactions **1 2** (positive effect) and **4 5** (positive effect), and the spray distance **2** with an effect of about $11\,HV_{0.3}$ per mm. Thus **1** > **1 2** ≥ **4 5** > **2** (absolute). The significant parameters for optimizing the lumped together-values of coating porosity and percent oxide were the traverse speed **4** with 0.38 % per mm per s, the two-factor interaction **2 3** (negative effect) and the plasma transferred arc current **5** with an effect per unit of −0.32 % per A. Thus **4** > **2 3** > **5** (absolute).

This result shows clearly the problems such coating property predictions have when performed at an insufficient level of predicting power, i.e. only two-level design: the quite different factor significances for microhardness and porosity precludes an unambiguous optimization treatment. Microhardness is presumably much affected by porosity but the parameter with the highest significance for the former, the plasma current **1** does not at all show up in the response polynomial of the latter. Likewise, the parameter with the highest significance for the porosity, the traverse speed **4** is not part of the response polynomial of the microhardness. With the large number of experiments expended (79) a folded-over, i.e. replicated three-level five-factor Box–Behnken design could have been executed with a slightly increased total number of runs of 92. This design allows for the estimation of nonlinear effects that are to be expected in the system. On the other hand, a result comparable to that de-

scribed above would have been obtained with a mere 24 runs as a reflected five-factor 12-run Plackett–Burman or L_{12} Taguchi design that estimates main effects clear of two-factor interactions with 6 unassigned factors for determination of the minimum factor significance. It should be emphasized again that in the interest of experimental economy it is good practice to always start with a simple screening to weed out the weakly significant parameters, and only than follow up with a full factorial design.

A simple two-level three-factor full factorial design 2^3 with 2 center points added was used by Troczynski and Plamondon [31] to optimize the erosion rate, Rockwell A-macrohardness, density, thermal decomposition of WC, and surface roughness of 88WC12Co coatings deposited by APS at a plasma power of 24 ± 4 kW on mild steel. The independent parameters and their levels were hydrogen content in % in the argon/hydrogen plasma gas **1** $\{(2; 4) \pm 0.3\%\}$, spray distance **2** $\{(51; 127) \pm 2.5\,\text{mm}\}$, and powder feed rate **3** $\{(30; 60) \pm 3\,\text{g min}^{-1}\}$. The choice of the independent parameters was as almost always a compromise, here between a limited experimental capability, a large number of variables potentially controlling the properties of the WC/Co coatings, and the practical relevance in industrial spraying operations. By plotting sections of the four-dimensional response hyperspaces $[\mathbf{1}, \mathbf{2}, \mathbf{3}, Y_i]$ it was possible to define a set of robust conditions that resulted in optimized coating properties (erosion rate $< 10\,\text{mg s}^{-1}$, hardness HRA > 40, density $> 9\,\text{g cm}^{-3}$, and W_2C content $< 7\%$ of initial amount of WC) insensitive to minor variations. These robust processing conditions were $\mathbf{1} = 2 \pm 0.5\%\,H_2$, $\mathbf{2} = 76.2 \pm 12.7\,\text{mm}$, and $\mathbf{3} = 60 \pm 10\,\text{g min}^{-1}$. With this highly economical design a set of operating windows were obtained as shown in Fig. 8-4.

Optimization of the porosity of APS-tungsten coatings on 6061 aluminum substrates was done using a combination of statistical designs [32], e.g. a full factorial 2^3 with 4 center points, and a central composite design using a 2^3 full factorial plus 6 star points and 2 center points. The variables were **1** = total gas flow, **2** = second-

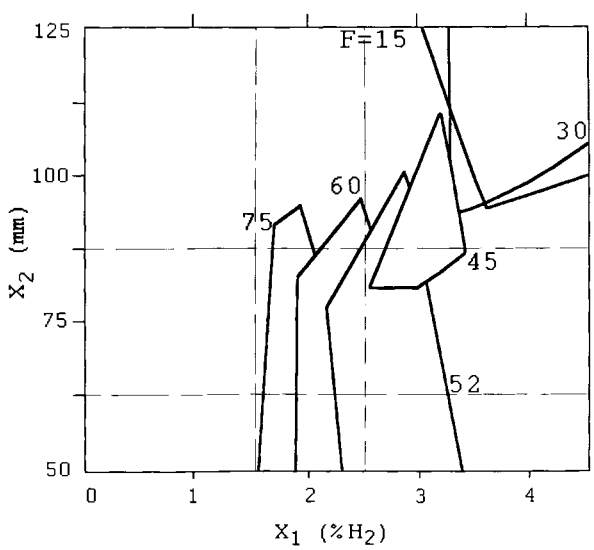

Figure 8-4. Response surface modification (RSM) optimization of an 88WC12Co coating to achieve an erosion rate $< 10\,\text{mg s}^{-1}$, Rockwell A hardness > 40, density $> 9\,\text{g cm}^{-3}$. Shown are operating windows of the hydrogen content of the plasma gas in % and the standoff distance in mm for powder feed rates F ranging from 15 to $75\,\text{g min}^{-1}$ [31].

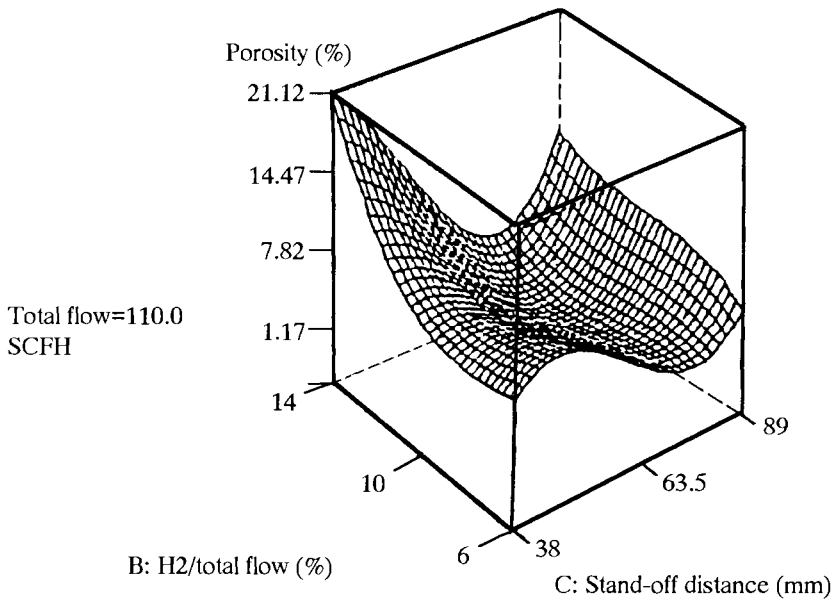

Figure 8-5. Optimization of the porosity of an APS–WC/Co coating on 6061 aluminum. The response surface of the porosity is displayed as a function of the ratio of the hydrogen/total gas flow (**2**), and the stand-off distance (**3**) for a total gas flow of 110 SCFH (approx. 3.1 $m^3 h^{-1}$) [32].

ary(H_2)-to-total gas flow ratio and **3** = stand-off distance. The average porosity measured ranged from 12.7 to 1.1%. The minimum porosity was obtained for **1** = 52 l min^{-1} (110 standard cubic feet per hour (SCFH)), **2** = 11%, and **3** = 70 mm (2.75″) as shown on the response surface (Fig. 8-5).

8.4.3 Fractional Factorial Designs

These designs permit a higher flexibility in terms of increasing the number of parameters under study. Although the number of plasma spray parameters that can potentially influence the coating properties is very large (≥ 150) it is common practice to consider only 8 to 12 parameters in statistical designs. Popular designs are 2^{8-4} fractional factorial designs of resolution IV.

8.4.3.1 Tungsten Carbide/cobalt Coatings

An example will be given of the optimization of 88WC12Co coatings deposited by APS (argon/helium plasma at Mach 2 velocities) onto low-carbon steel [33]. The eight selected parameters and their ranges were the plasma current **1** (700; 900 A), argon gas pressure **2** (0.34; 1.36 MPa), helium gas pressure **3** (0.34; 1.36 MPa), powder gas pressure **4** (0.34; 0.68 MPa), powder feed rate **5** (0.5; 2 scale value), powder

grain size **6** ($-45+5$; $-75+45\,\mu m$), number of traverses **7** (5;15 for set 1 and 20;30 for set 2) and spray distance **8** (250; 450 mm). If all possible experiments would be executed, their total number would be 256 (2^8). In the present situation, however, only a fraction of the total, i.e. the 1/16 replicate was selected (2^{8-4}). Two sets of 16 spray runs each were performed. During the first set, the number of traverses was varied between 5 and 15; this produced relatively thin coatings with a maximum thickness of 80 μm. The data from this set were statistically evaluated to yield information on the main factor effects and synergistic two-factor interactions. The second set with the number of traverses varying between 20 and 30 resulted in coatings with a maximum thickness of 200 μm. The data from the second set were used to evaluate the microhardness and the cohesive strength of the coatings. The design allows the calculation of the eight main effects clear of the composite two-factor interactions E_i. The calculations are executed in Appendix C.

The statistical significance of the factor effects calculated analogous to the simple procedure outlined in Sec. 8.3.2 (see Appendix C) was checked against the minimum factor significance, $\{\min\} = \sigma_{FE} \times t_\nu^\alpha$, where $\sigma_{FE} = (1/n \sum E_i^2)^{1/2}$, t_ν^α is the Student's t-value for a confidence level α of a double-sided significance test and $\nu =$ degrees of freedom. All absolute factor effects larger than or equal to $\{\min\}$ were considered to be significant.

The composite two-factor interactions E_i were calculated in a similar fashion (see Appendix C). They are the unassigned factors that can be used to estimate the experimental error, i.e. the σ_{FE} value needed to calculate the minimum factor significance, $\{\min\}$. With the data obtained it follows that $\sigma_{FE} = (1/n \sum E_i^2)^{1/2} = (3592/7)^{1/2} = 22.6$, and $\{\min\} = 22.6 \times t(\alpha = 0.90, \nu = 7) = 22.6 \times 1.895 = 43$. This means, that all main factor effects whose absolute values are larger than 43 should be considered significant at a confidence level of 90%. Checking with the data in Appendix C, this is the case for $\mathbf{5} = 54$ and $\mathbf{6} = 55$ for thicker coating, i.e. those obtained from the second set of experiments with the number of traverses ranging between 20 and 30. Both effects have positive signs, i.e. the thickness of the coating increases with increasing powder feed rate, **5** and increasing spray distance, **8**. Short spray distances lead to overheating of the alloy powder thus causing thermal decomposition and/or reaction of the WC with the cobalt metal matrix forming η-carbides Co_nW_mC (Fig. 5-17; [34]). Hence, the response polynomial of the thickness of plasma-sprayed 88WC12Co alloy coatings can be approximately expressed by the equation $d(\mu m) = 32 + 27X_5 + 28X_8$. For thinner coatings a slightly different picture emerges. In this case the significant factors affecting coating thickness are **6** (negative effect) > **8** > E_4, E_6 (negative), E_5 > **7** > **3**; Fig. 8-6 shows the position of the experimental data points for the coating thickness in μm in a four-dimensional hypercube where the four axes of the cube are the factors **6**, **7**, **8** and **3**. The design consists of two nested cubes with $\mathbf{3} = -1$ and $\mathbf{3} = +1$. These 3D-cubes are also shown in Fig. 8-6 (bottom). Maximum thickness of the coatings can be obtained using fine powders, long spray distances, and high helium gas pressure. The complex statistical significance of the composite two-factor interactions $E_4 = \mathbf{15} + \mathbf{38} + \mathbf{26} + \mathbf{47}$, $E_5 = \mathbf{16} + \mathbf{78} + \mathbf{34} + \mathbf{25}$, and $E_6 = \mathbf{17} + \mathbf{23} + \mathbf{68} + \mathbf{45}$ may be somewhat deconvoluted by assuming that there exists at least one large component interaction involving factors with significant main effect in each composite interaction.

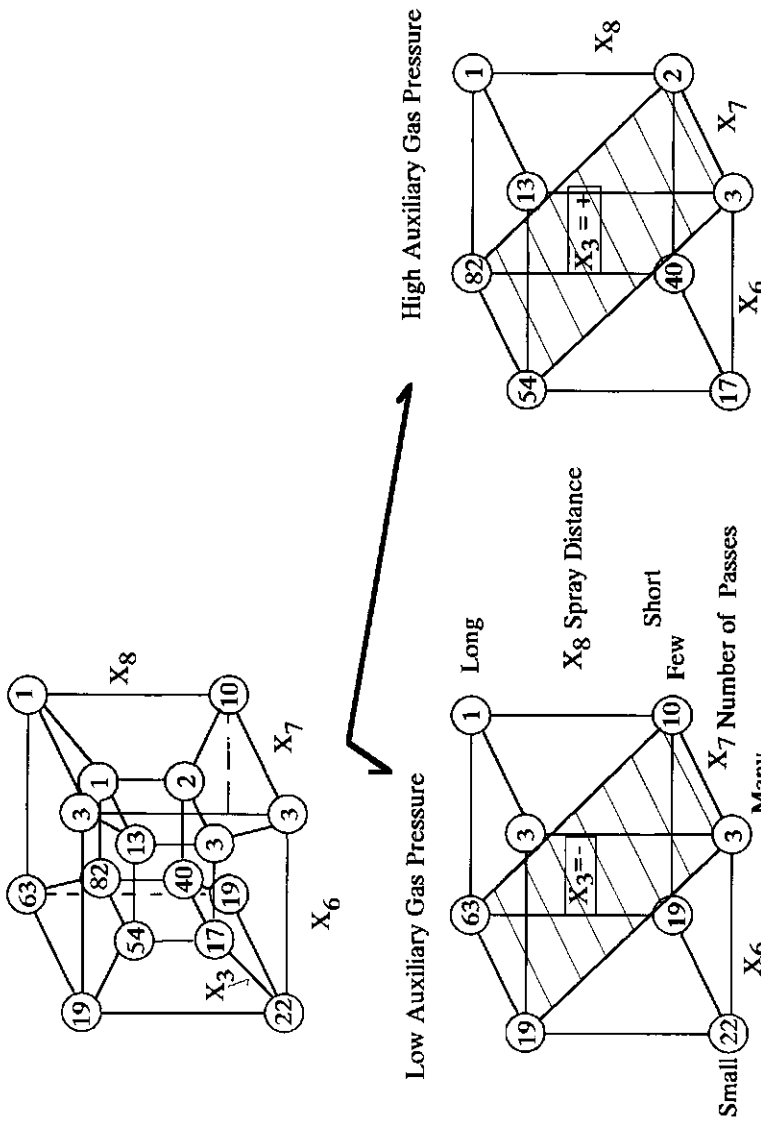

Figure 8-6. 4D-hypercube of optimization of the thickness of 88WC12Co coatings as a function of the auxiliary (helium) gas pressure **3**, the powder grain size **6**, the number of traverses **7**, and the stand-off distance **8** [33].

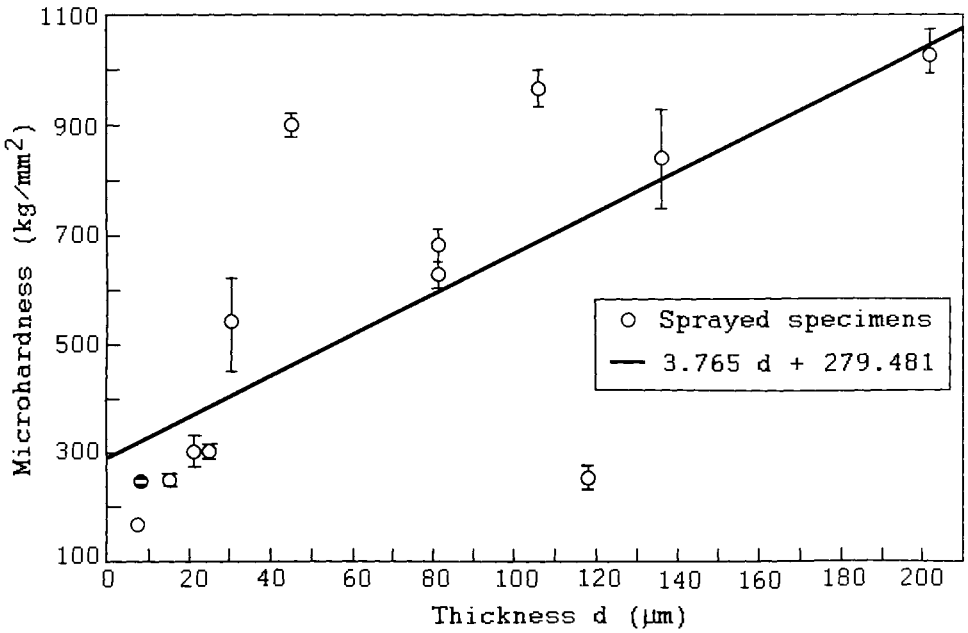

Figure 8-7. Quasi-linear relationship between microhardness ($HV_{0.2}$) and thickness for 88WC12Co coatings [33].

The most likely candidates are **38** for E_4, **78** for E_5, and **68** for E_6. Additional experiments with a larger set of runs at a higher power of prediction would be required to resolve these ambiguities.

For the microhardness there exists only a weak significant factor, **8**. There is a quasi-linear relationship between coating thickness and microhardness (Fig. 8-7). The maximum microhardness obtained for coatings with thicknesses exceeding 200 µm is 1200 $HV_{0.2}$ (75 HRC). The cohesive strength of the coatings exceeded 60 ± 16 MPa and yielded a maximum value of 80 MPa. Additional scanning electron microscopy investigations were performed to obtain qualitative information on the porosity. The only significant parameter to describe the development of porosity is the powder grain size, **6**, i.e. fine powders produce higher coating porosity. Statistically nonsignificant results were obtained for the degree of densification; high plasma currents, **1** and a small powder grain size, **6** produced a higher degree of densification. These results are somewhat contradictory as increased densification should also produce a lower porosity. It may be, however, that overheating of the particles at short stand-off distances leads to vaporization, and the increased porosity simply reflects the eruption of gaseous decomposition products such as CO_2 generated by partial oxidation of tungsten carbide under formation of η-carbides [34].

In conclusion, the application of the statistical design matrix 2^{8-4} to 88WC/12Co coatings showed that the eight parameters selected as variables can be divided into highly significant ('soft'), and less or insignificant ('hard') parameters that can be

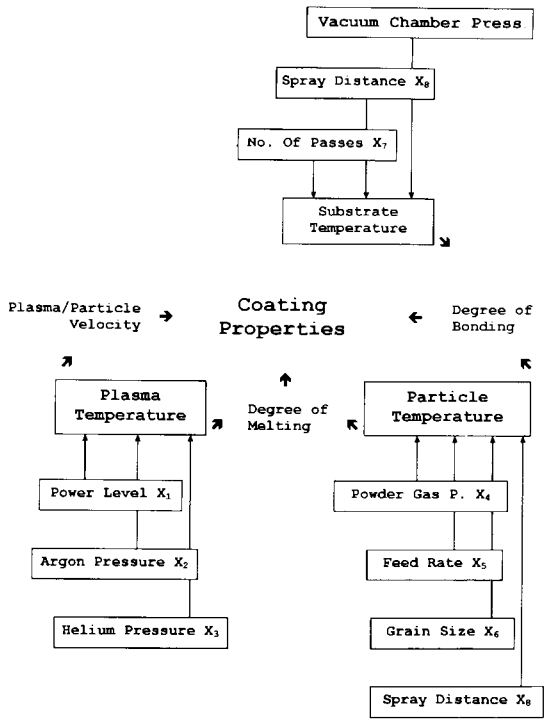

Figure 8-8. Plasma spray parameters **1** to **8** show a three-tiered hierarchy: plasma/particle velocity, degree of melting, and degree of bonding [33].

varied widely (see [31]). 'Soft' parameters for optimizing coating thickness are powder grain size and spray distance, i.e. parameters that determine the degree of melting of the particles. Typical 'hard' parameters are argon gas pressure, powder gas pressure and powder feed rate.

Figure 8-8 shows the three-tiered hierarchy of the selected plasma spray parameters. Third-level parameters are plasma/particle velocity, degree of particle melting, and degree of bonding of the coating to the substrate. These properties are influenced by the second-level parameters plasma temperature, particle temperature and substrate temperature. These in turn are determined by the eight first-level input parameters. This scheme illustrates once more that the fact that these parameters do not always act in the same directions (saddle points of the response surface), requires statistical multifactorial design to unravel the generally complex parameter interactions.

8.4.3.2 Ferrosilicon Coatings

A second case study concerns the optimization in terms of coating thickness and microhardness of an 85Fe15Si (Valco 3603.0, $-22 + 5\,\mu m$) coating on carbon steel [35]. This material is known for its excellent corrosion resistance and may have applications in demanding environments such as those present in coal gasification where hydrogen sulfide leads to severe stress corrosion cracking. Samples were cut

from St 37 steel plate and mounted on a specially designed sample holder that permits cooling by water flowing through a thin copper pipe attached by hard soldering to the underside of the sample holder. The plasma spray equipment used to deposit the coatings was a conventional METCO system with a vibrating hopper, and a METCO 9M plasmatron. Spraying was performed with an argon/hydrogen plasma gas. A fractional factorial design 2^{8-4} was selected whose factors and their levels were as follows: **1** plasma current (300;500 A), **2** argon gas flow (100;140 scale value), **3** hydrogen gas flow (2;4 scale value), **4** substrate cooling[3] (no;yes), **5** ammonia shroud[4] (no;yes), **6** traverse speed (20;30 m min^{-1}), **7** substrate roughness (0.45; 1.1 μm), and **8** stand-off distance (80;120 mm). Constant factors were the anode (GH 732), powder feed tube (A), powder spray nozzle (2), powder feed rate (60 g min^{-1}), number of preheating cycles (3), number of spray traverses (3) and overlap (5 mm). The main factor effects **1** to **8** as well as the composite two-factor interactions E_1 to E_7 were estimated for the coating thickness (Y_1) and the microhardness (Y_2). The significant main effects for coating thickness were **4** (negative) and **6** (positive), i.e. the coating thickness is maximized (175 μm) on a preheated substrate with increasing traverse speed. There is a conspicuously large negative composite two-factor interaction, $E_2 = \mathbf{13} + \mathbf{27} + \mathbf{46} + \mathbf{58}$ (see Appendix C). This can be rather easily explained by the large value of the (negative) **46** two-factor interaction involving the two significant main effects **4** and **6**.

The significant main effects for the microhardness were **3** (positive), **4** (negative) and **8** (negative), i.e. the microhardness is maximized (325 kPa) at a short stand-off distance on a preheated substrate with increasing hydrogen flow rate (plasma enthalpy). Since it could be shown that for the optimization of the microhardness only three of the original eight selected parameters were significant, the 2^{8-4} fractional factorial design can be reduced to a replicated 2^3 full factorial design in variables **3**, **4** and **8**. Hence the assumption has been made that the remaining factors are essentially inert. However, the rather large standard deviation of the replicated microhardness values showed that this simplifying assumption cannot be upheld. For example, **1** is almost at the level of significance and may account for the variation of the replicated values. Thus the factor **1** behaves like a perturbation of the 3D-response surface in **3**, **4** and **8**, and it must be concluded that larger plasma arc currents, i.e. higher plasma temperatures will also increase the microhardness of 85Fe15Si coatings. Plotting the microhardness in a 4D-hypercube design (Fig. 8-9) in **1**, **3**, **4** and **8** shows clearly that the associated response surface has a saddle in the **34** plane for low and high level variations of **1**.

In conclusion, optimized microhardness values for 85Fe15Si coatings can be obtained by:

- substrate preheating,
- increased flow rate of high-enthalpy gases, e.g. hydrogen,

[3] 'No' substrate cooling means substrate preheating.

[4] Ammonia was used as a shroud gas since the 85Fe15Si coating was developed as a bond coat for a plasma-sprayed silicon nitride-based high temperature erosion resistant coating. Ammonia was supposed to counteract the thermal decomposition of silicon nitride during spraying [35].

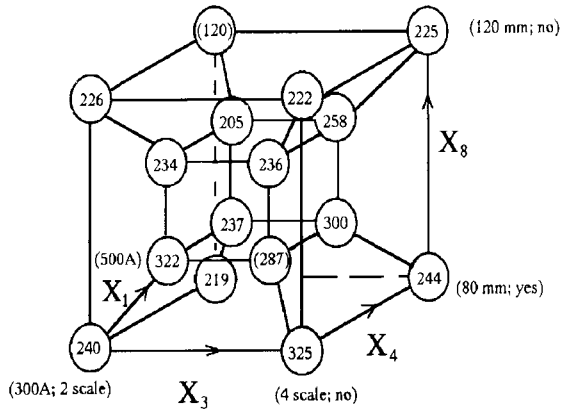

Figure 8-9. Geometric 4D-representation of a 2^{8-4} design in variables **1**, **3**, **4** and **8** to estimate the microhardness of a 85Fe15Si coating. The numbers refer to $HV_{0.2}$ values in kPa [35].

- short stand-off distances, and
- high plasma arc current.

Under these conditions the porosity of the coatings will also be minimized, and adhesion to the substrate will be maximized.

8.4.3.3 Alumina/titania Coatings

Similar coating optimization has been performed for alumina–titania plasma-sprayed coatings applied to pump plungers operating at elevated temperature and as protective coatings against hot gas erosion of petrochemical processing equipment [36]. As above, a 2^{8-4} fractional factorial design of resolution IV was selected with **1** plasma current (850;950 A), **2** argon gas pressure (345;517 kPa), **3** helium gas pressure (276;414 kPa), **4** substrate preheating (23;200 °C), **5** powder feed rate (4.5;5.5 r.p.m.), **6** roughening grit size (80;40 mesh), **7** number of traverses (20;50) and **8** stand-off distance (76;127 mm). Coating thickness was found to be significantly influenced by **2**, **7** and **8**. Figure 8-10 shows the 2^3 design cube with the results of the replicated coating thickness measurements. Figure 8-11 shows a different way to express parameter significance. The coefficients obtained by calculation identical to those shown in Appendix C have been plotted on a probability net. If the coefficients would only vary in a random fashion then their plot should give a straight line (Gaussian distribution). Deviation from this straight line signifies significant parameter effect. Figure 8-11 shows that the thickness of alumina–titania (97/3) coatings is significantly influenced by the argon gas pressure, **2** and the spray distance, **8** in a negative way, but positively influenced by the number of passes, **7**, the powder feed rate, **5** and a two-factor composite interaction, E_3 (positive effect) whose determining contributions are presumably the two-factor interactions **28** and **57**. In Fig. 8-12 it is shown that the interaction **28** has a large difference in slope at low and high levels of **7** with a cross-over at high **7**. On the other hand, the probability plots of the coefficients of the second-order polynomial response equations for the microhardness (Vickers test, $HV_{0.3}$; Fig. 8-13) and the abrasion mass loss determined

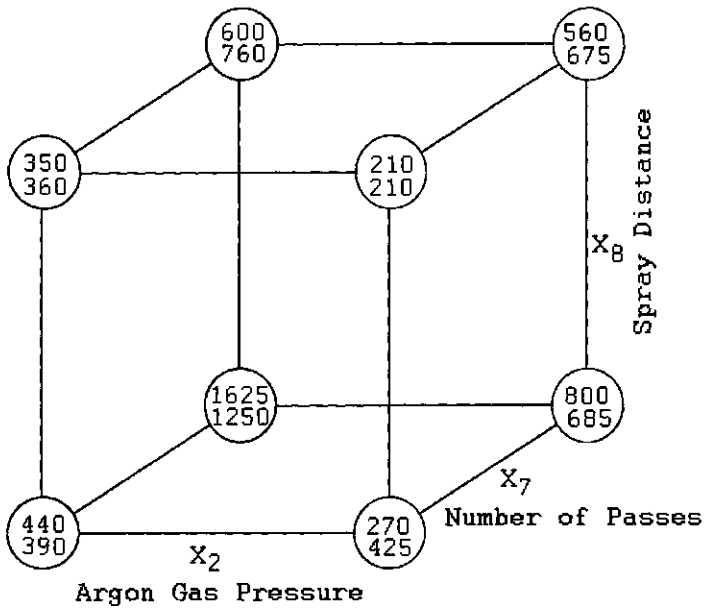

Figure 8-10. Optimization of the thickness of alumina/titania coatings as a function of argon gas pressure **2**, number of traverses **7**, and stand-off distance **8** [36].

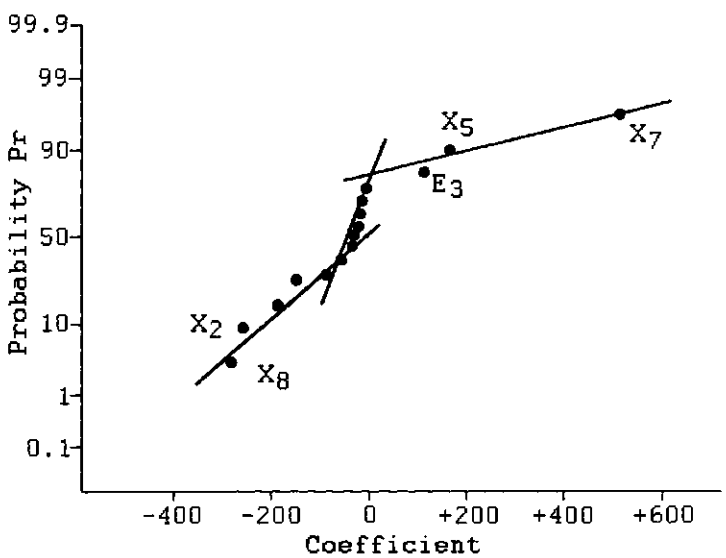

Figure 8-11. Probability distribution of the coefficients of the polynomial equation obtained for the thickness of alumina/titania coatings [36].

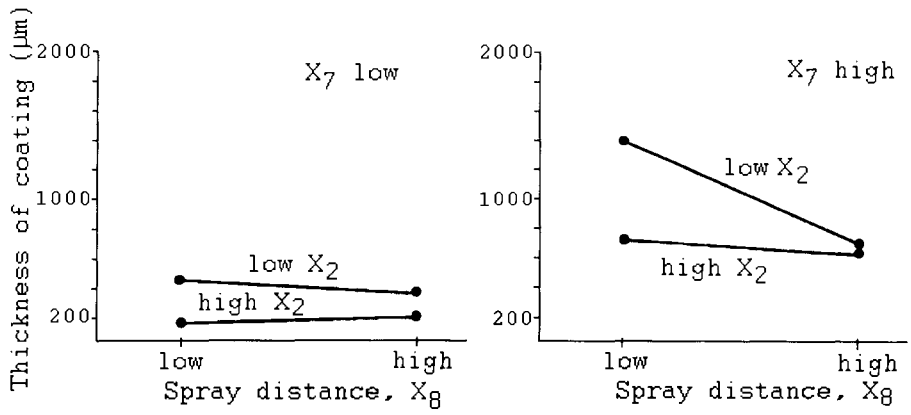

Figure 8-12. The two-factor interaction **28** is negligible for few traverses ($7 < 20$) but strong for many traverses ($7 > 50$) [36].

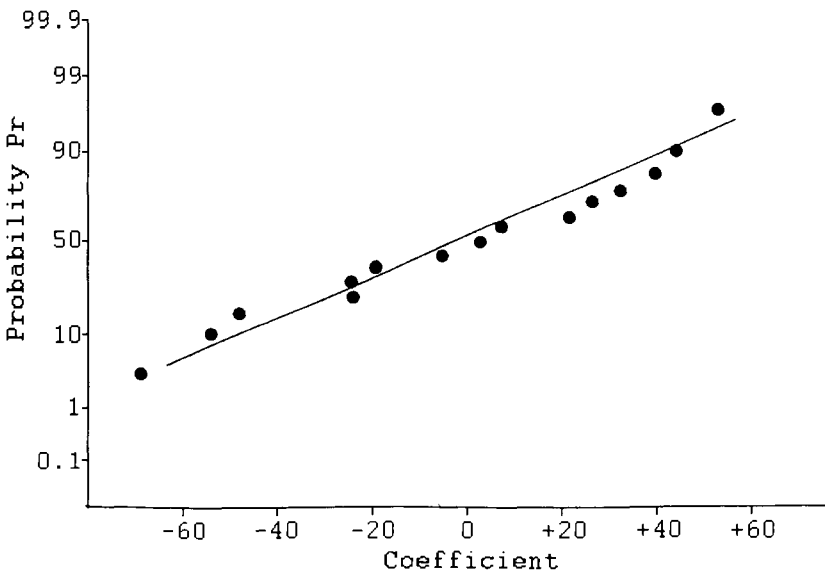

Figure 8.13. Probability distribution of the coefficients of the polynomial equation obtained for the microhardness of alumina/titania coatings, showing random, i.e. statistically nonsignificant factor effects [36].

by the ASTM G 65 test (Fig. 8-14) show random behavior thus indicating that in both cases the properties are not significantly influenced by the selected factors. The microhardness increases linearly (correlation factor 0.61) with coating thickness according to a limiting equation $HV_{0.3} = ad + b$, where $a = 120\,kg\,mm^{-3}$, $b = 974\,kg\,mm^{-2}$, and $d =$ thickness (mm). The abrasion mass loss is inversely proportional (correlation factor -0.89) to the coating thickness and obeys the equa-

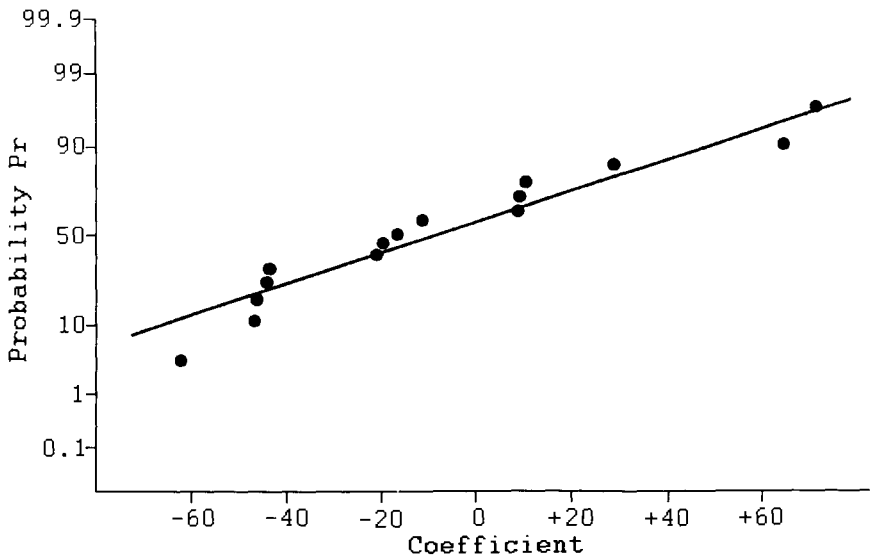

Figure 8-14. Probability distribution of the coefficients of the polynomial equation obtained for the abrasion mass loss (ASTM G65) of alumina/titania coatings, showing statistically nonsignificant factor effects [36].

tion $\Delta m = c/d$ where $c = 45.3\,\mathrm{mg\,mm^{-1}}$ and $d =$ thickness (mm). Figure 8-15 shows that there is also an inverse relationship between abrasion mass loss and microhardness that can be expressed by the power function $\Delta m = A(\mathrm{HV}_{0.3})^{-B}$ [kg] where $A = 4.3 \times 10^{24}$ and $B = 9.5$ (correlation factor -0.64).

In conclusion, application of a two level fractional factorial design 2^{8-4} to a set of $97Al_2O_33TiO_2$ coatings on low-carbon steel (A 569) surfaces showed that the eight parameters selected could be divided into highly significant or 'soft', and less or nonsignificant 'hard' parameters. 'Soft' parameters to describe the coating thickness are the stand-off distance **8**, the number of traverses **7**, and the argon gas pressure **2**. Typical 'hard' parameters are arc current, preheating temperature and grain size of the grit blasting material.

8.4.3.4 Stellite Coatings

Another example deals with stellite 6 (28Cr1C4W1Si, bal. Co) coating deposited by a PTA surfacing process on mild steel (SIS 2172) bars by Herrström *et al.* [37]. A 2^{6-2} fractional factorial design was used in the parameters, **1**, plasma current (100;130 A), **2**, argon gas flow ($1;3\,\mathrm{l\,min^{-1}}$), **3**, powder gas flow ($2;4\,\mathrm{l\,min^{-1}}$), **4** oscillation frequency ($82;90\,\mathrm{min^{-1}}$), **5** weld speed ($5;7\,\mathrm{cm\,min^{-1}}$) and **6** stand-off distance (6;14 mm). Dependent parameters estimated were the percentage dilution, the hardness HV_{30}, and the width and the height of the deposit in mm. The hardness of the PTA deposit depends significantly with $\mathbf{2} > \mathbf{6} > \mathbf{1} \gg \mathbf{16} + \mathbf{45}$, the width of the de-

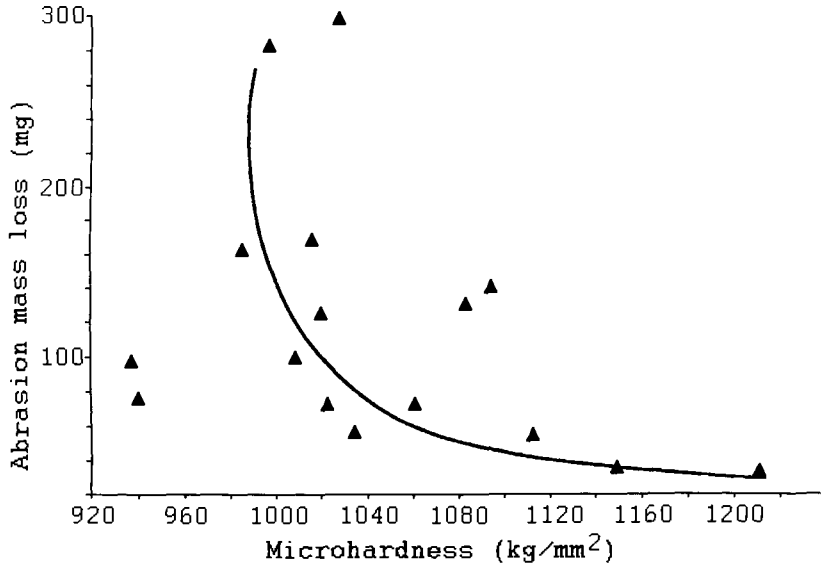

Figure 8-15. Inverse relationship between abrasion mass loss and microhardness of alumina/titania coatings [36].

posit shows **4** > **2**, and the height **1** > **2**. The dilution depends significantly at a confidence level < 95% on the parameters **2** > **1** ≫ **6**. It should be mentioned that the responses Y are not independent of each other. So the hardness depends not only on the dilution but also on the microstructure and the cooling rate that were not explicitly parts of the experimental design. At the working point, i.e. at an intermediate parameter level ('0') the following optimized responses were found: hardness $424.6 \pm 3.78\,HV_{30}$, dilution $6.84 \pm 0.64\%$, width 15.24 ± 0.30 mm, and height 2.84 ± 0.29 mm.

8.4.3.5 Titanium Coatings

Work by Lugscheider *et al.* [38] on vacuum plasma-spraying of Ti coatings on 1.4571 and 1.4541 austenitic steel substrates employed an L_8 Taguchi matrix with four parameters varied. These parameters and their levels were the plasma current **1** (605; 655 A), argon gas flow **2** (33; 43 standard liter per minute (SLPM)), vacuum chamber pressure **4** (144; 164 mbar) and powder feed rate **6** (6.8; 10.8 g min^{-1}). The parameters **3** (hydrogen gas flow; 6.5 SLPM), **5** (spray distance; 280 mm), **7** (plasma transferred arc current; 0 A) and **8** (sputter distance 320 mm) were kept constant at the levels indicated. The eight runs performed actually constitute an 2^{8-5} matrix. Two additional runs with parameters **1** and **2** changed in the directions indicated by the fractional factorial design, and parameters **4** and **6** kept at their zero levels, i.e. midway between the upper and lower parameter levels led to the desired minimum porosity of 1.3% [39]. The other optimized dependent parameters were the micro-

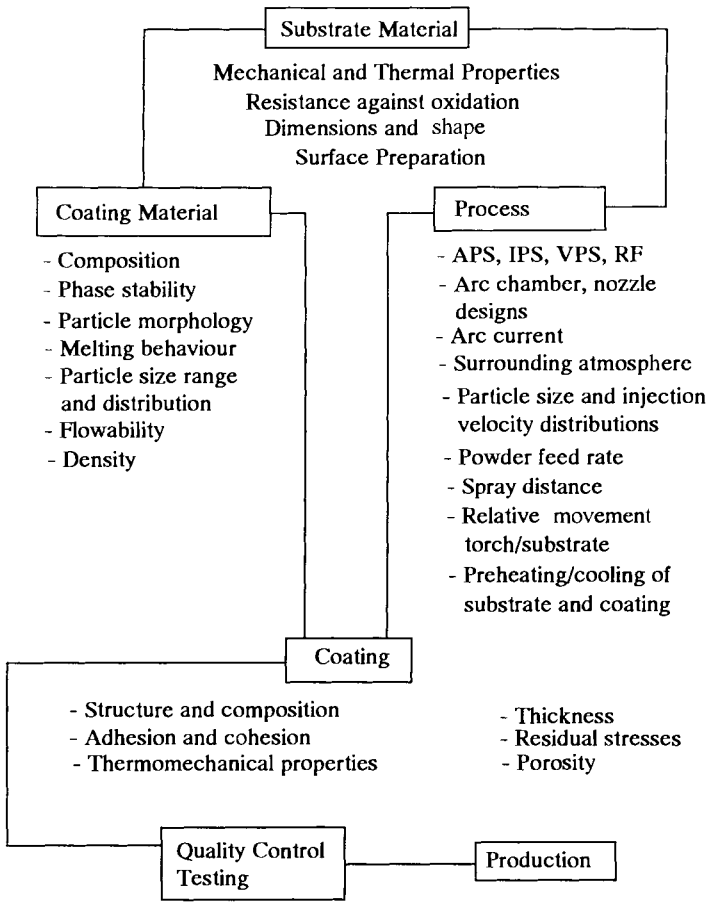

Figure 8-16. Main aspects of plasma spraying considering substrate–coating–process interactions.

hardness ($218 \pm 37\,HV_{0.05}$), adhesion strength obtained by DIN 50 160 ($75 \pm 4\,N\,mm^{-2}$), and the traverse bending strength by DIN 50 111. The significant parameters for this optimization were **2** (negative effect) $\gg$ **14** $>$ **1**.

8.5 Future Developments

Figure 8-16 shows the main aspects of plasma spraying that have to be considered in order to produce advanced metal, ceramic or composite coatings with high in-service performance. Most of the aspects listed therein have been dealt with rather exhaustively.

Thermal spray research and development of advanced materials for high performance applications is increasing rapidly, and many developments are being commercialized now. As an indication of this rapid development it should be mentioned that over 80% of the advances that have been made over the last 80 years have been made in the last two decades! Equipment and process advances have typically led the technology in the past. Increasingly, materials and process control (SPC), and novel applications will lead in the next 10 years.

Future developments in the advanced materials coating field can be characterized and evaluated in terms of their economic feasibility by looking at different technology support and development strategies [40]. Figure 8-17 shows that wear and thermal barrier coatings are level I strategies that deploy current technologies to improve the competitive performance of small companies or create new companies. Bioceramic and diamond coatings are level II strategies that focus on the development of innovative applications of new technological discoveries. Finally, low friction coatings, high-temperature superconducting, and silicon nitride coatings are level III strategies whose efforts are still concentrated on basic research leading up to the discovery of new technologies. Those new technological breakthroughs expected for the future will predominantly assist large companies, and attract completely new industries [43].

The main areas of contemporary developments will be automotive coatings with high rate, low cost processing, while aerospace applications are triggering the advance of the technology for novel thermal barrier coatings, spray forming and composite materials processing.

Advances are being typically made in the following areas [41]:

- materials, process, and equipment;
- control devices and automated robotic handling;
- use of SPC with resulting close process monitoring;
- accumulation of data bases and development of expert systems;
- HVOF processing;
- engineered powder production; and
- composite and intermetallic spray forming.

Thermal spray processing education and training needs to be implemented and managed on a broader base. Collaboration with industry in the resource and manufacturing sectors will lead increasingly to strategic alliances that enable industry to produce more competitively and environmentally compatibly. Process control, including modeling of complex plasma–particle–substrate interactions, on-line process diagnostics, and development of novel coatings with improved performance are areas rich in research needs and opportunities.

Such areas can be predicted by application technology mapping [42]. Marketers look for applications of materials, and then determine the performance needs for particular applications. These data are mapped against the value-in-use estimate and the customer's ability to pay (Fig. 8-18). The *military* have clearly a high ability to pay for sophisticated materials and coatings, or products with a high value-in-use, for example piezoelectric, ferroic and superconducting coatings for range finders and

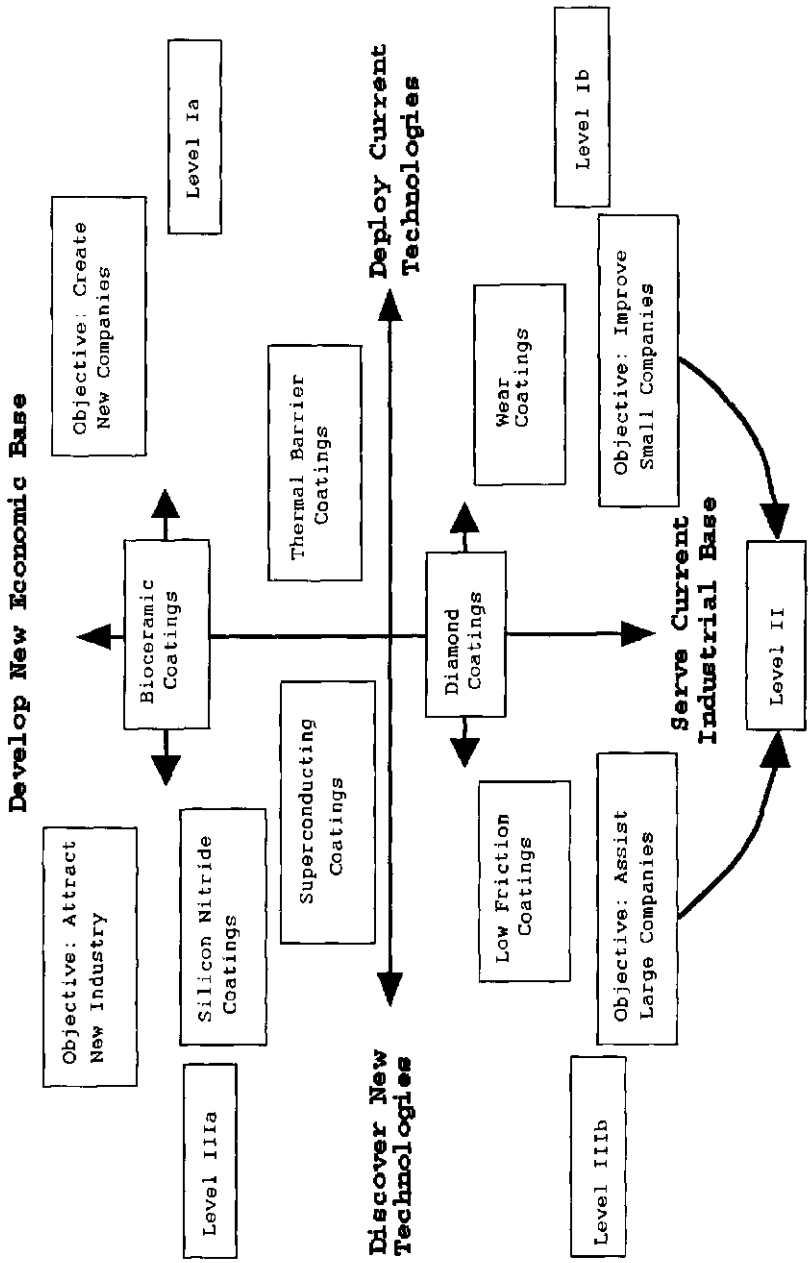

Figure 8-17. Technology support and development strategies applied to various types of coatings [43].

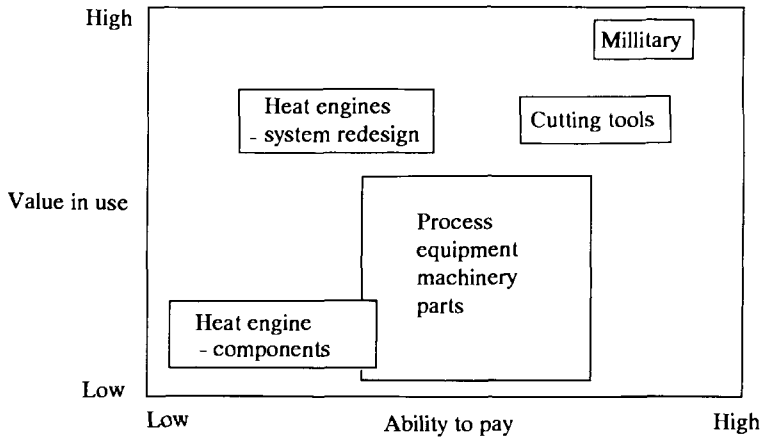

Figure 8-18. Application technology mapping for coatings [42].

surveillance systems. Titanium nitride, titanium carbide, and diamond coatings for ceramic *cutting tools* are high-value-added but nevertheless cost-competitive because of their superior wear performance in numerically controlled high-speed machining of tough and hard steels, and superalloys. On the other hand, *heat engine components* such as ceramic turbochargers, thermal barrier coatings (TBCs) and a variety of automotive sensors based on functional ceramic coatings and thin films have a low value, and the ability to pay for it by the car manufacturer is also low in order to maximize profit. New developments are presently being considered such as thick thermal barrier coatings (TTBCs) for diesel engines to replace water cooling by air cooling systems. The middle ground of Fig. 8-18 is occupied by wear-resistant parts for nonautomotive markets, i.e. *process equipment and machine tools.* In this area a new strong driving force is evolving that is geared towards first-generation materials to improve process efficiency and overall productivity in the manufacturing and resource industries [43].

In conclusion, the future of advanced materials coatings applied by plasma spray technology looks very bright. There are, however, problems still to be solved.

Technical problems include optimization of plasmatron design, powder size and composition, rheological and flow properties of powders, overspray losses and surface preparation. Quality control procedures must be developed or improved, and implemented for ceramic, metal and composite coatings to standardize impact testing, hardness testing, shear and bending testing, cavitation-erosion testing, slurry abrasion testing etc. Most of all, reliable and reproducible tests must be developed to measure the adhesion strength of the coatings to the substrate. Finally, the development of computer codes is necessary that model the forces acting on the coating/substrate interface. The objective is to develop coatings that sustain in-film compressive loads during service, thus improving adherence to the substrate and, in turn, maximizing the service life of the coated equipment.

There is also the considerable challenge of improving the image of thermal spray

coatings as a viable, reliable und immensely versatile option available to design engineers. Although it is widely recognized that plasma-sprayed coatings can provide many successful answers to engineering problems, its level of awareness in industry and government has to be raised [43].

Thermal spray technology is emerging as an important tool of increasingly sophisticated surface engineering technology. Initially developed as a simple and relatively crude surfacing tool, thermal and plasma spraying, respectively is now considered a powerful and flexible materials processing method with a high potential of development [44]. It appears that the return on investment in this area of surface engineering is excellent, and that small and medium-sized enterprises can hugely benefit from entering a market segment that by many is considered the *materials technology of the 21st century!*

At the end of this treatise on plasma-sprayed coatings the following final statement should be made. Strict quality control of well established coatings, and close attention to the design and testing of coating/substrate systems as a single synergistic entity, combined with the development of novel structural and functional coatings using improved automated equipment and comprehensive data bases and expert systems, will secure plasma spray technology a substantial market niche in the immediate future beyond the year 2000.

References

[1] H. Holleck, *Surf. Eng.* **1991**, *7*, 137.
[2] S. Sampath, H. Herman, N. Shimoda, T. Saito, *MRS Bull.* **1995**, *January*, 27.
[3] D. B. Marshall, T. Noma, A. G. Evans, *Commun. Am. Ceram. Soc.* **1982**, *65*, C-175.
[4] S. Bisgaard, *Proc. 3rd NTSC*, Long Beach, CA, USA, 20–25 May **1990**; p. 661.
[5] R. B. Heimann, *Proc. First All-Alberta Appl. Stat. Biometr. Workshop. AECV91-P1*, Edmonton, Alberta, Canada, 18–19 October **1990**, p. 87.
[6] E. Lugscheider, M. Knepper, DVS, Düsselderf **1991**, *136*, p. 88.
[7] R. L. Plackett, J. P. Burman, *Biometrika* **1946**, *33*, 305.
[8] G. E. P. Box, D. W. Behnken, *Technometrics*, **1960**, *2*, 455.
[9] G. E. P. Box, W. G. Hunter, J. S. Hunter, *Statistics for Experimenters*, Wiley, NY, USA, **1978**.
[10] W. E. Deming, *Out of the Crisis*, MIT Press, Cambridge, MA, USA, **1986**.
[11] G. Taguchi, S. Konishi, *Taguchi Methods, Orthogonal Arrays and Linear Graphics*, American Supplier Institute, **1987**.
[12] P. Whitcomb, *Design-Expert*™, version 3.0, Stat-Ease Inc., 2021 East Hennepin, #191, Minneapolis, MN 55413.
[13] J. W. Tukey, *Ann. Math. Stat.* **1962**, *33*, 1.
[14] C. Daniel, *Applications of Statistics to Industrial Experimentation*, Wiley, NY, USA, **1976**.
[15] W. G. Cochran, G. M. Cox, *Experimental Designs*, Wiley, NY, USA, **1957**.
[16] DuPont de Nemours & Co, *Strategy of Experimentation*, **1975**.
[17] E. De Bono, *The use of Lateral Thinking*, Penguin Books, Harmondsworth, **1970**.
[18] H. Bandemer, A. Bellmann, *Statistische Versuchsplanung*, 4th ed., Teubner, Stuttgart, Germany, **1994**, p. 133.
[19] S. I. Satterthwaite, *Technometrics* **1959**, *1*, 111.
[20] G. E. P. Box, N. R. D. Draper, *Empirical Model Building and Response Surface Methodology*, Wiley, NY, USA, **1987**.

[21] F. Yates, *The Design and Analysis of Factorial Experiments*, Imperial Bureau Soil Sci., Techn. Commun., **1937**, 35.
[22] J. S. Hunter, *Technometrics* **1966**, *8*, 177.
[23] G. E. P. Box, J. S. Hunter, *Technometrics* **1961**, *3*(3), 311.
[24] G. E. P. Box, K. B. Wilson, *J. Roy. Stat. Soc. B* **1951**, *13*, 1.
[25] S. Thiele, Mikrohärte, Mikrostruktur und Haftung vakuum-plasmagespritzter TiC/Mo_2C/Ni, Co-Verbundschichten. Unpublished diploma thesis, Freiberg University of Mining and Technology, June **1994**.
[26] E. R. Novinski, A. J. Rotolico, E. J. Cove, *Proc. 3rd NTSC*, Long Beach, CA, USA, 20–25 May **1990**; p. 151.
[27] T. Chon, A. Aly, B. Kushner, A. Rotolico, W. L. Riggs, *Proc. 3rd NTSC*, Long Beach, CA, USA, 20–25 May **1990**; p. 681.
[28] J. E. Nerz, B. A. Kushner, A. J. Rotolico, *Proc. 3rd NTSC,* Long Beach, CA, USA, 20—25 May **1990**, p. 669.
[29] J. Walter, W. L. Riggs, *Proc. 3rd NTSC*, Long Beach, CA, USA, 20–25 May **1990**, p. 729.
[30] T. C. C. Hurng, M. B. C. Quigley, R. L. Apps, *Proc. 2nd Int. Conf. on Surface Engineering*, Stratford-upon-Avon, UK, 16–18 June **1987**, p. 413.
[31] T. Troczynski, M. Plamondon, *J. Therm. Spray Technol.* **1992**, *1*(4), 293.
[32] D. J. Varacalle, L. B. Lundberg, B. G. Miller, W. L. Riggs, *Proc. 14th ITSC'95*, Kobe, Japan, 22–26 May **1995**, p. 377.
[33] R. B. Heimann, D. Lamy, T. Sopkow, *J. Can. Ceram. Soc.* **1990**, *59*(3), 49.
[34] K. Hajmrle, M. Dorfman, *Mod. Dev. Powder Metall.* **1985**, *15/17*, 409.
[35] R. B. Heimann, *Development of Plasma-Sprayed Silicon Nitride-Based Coatings on Steel*, Research Report to NSERC and EAITC, Canada, 15 December **1992**.
[36] R. B. Heimann, D. Lamy, T. N. Sopkow, *Proc. 3rd NTSC*, 20–25 May **1990**, Long Beach, CA, USA, p. 491.
[37] C. Herrström, H. Hallén, A. Ait-Mekideche, E. Lugscheider, *Proc. TS'93*, Aachen **1993**, DVS 152, p. 409.
[38] E. Lugscheider, P. Lu, B. Hauser, D. Jäger, *Surf. Coat. Technol.* **1987**, *32*, 215.
[39] E. Lugscheider, P. Lu, *Proc. Int. Conf. Plasma Science Technol.*, Beijing, China, 4–7 June 1986; Science Press, Beijing, China, **1986**, p. 250.
[40] Center for Economic Competitiveness. *Assessment of Alberta Technology Centers*. SRI International, **1990**.
[41] R. W. Smith, R. Novak, *PMI*, **1991**, *23*(4), 231.
[42] S. K. Sutliff, *Trans. 4th Workshop CUICAC*, Toronto, Ontario, Canada, 25–26 May **1987**.
[43] R. B. Heimann, *Proc. Adv. Mater.* **1991**, *1*, 181.
[44] E. Lugscheider, H. Eschnauer, U. Müller, Th. Weber, *PMI*, **1991**, *23*(1), 33.